Progress In Electromagnetics Research C, Vol. 129, 203–219, 2023

Low Profile Design of Regular Shape Microstrip Antennas Backed by Fractal Slots Cut Ground Plane for Circular Polarized Response

Aarti G. Ambekar and Amit A. Deshmukh*

Abstract—Thinner substrate designs of square and circular microstrip antennas using fractal variations of U-shape and half U-shape slot cut ground plane are proposed for circularly polarized response. The 1st, 2nd, and 3rd order fractal variations of slots on the ground plane are studied. The fractal slot cut variations degenerate patch fundamental mode into dual orthogonal resonant modes, and an optimum spacing between them yields circularly polarized characteristics. Amongst all the designs, circular microstrip antenna using the 1st order fractal U-slot design yields the optimum result. It offers axial ratio bandwidth of 60 MHz (2.14%) with a broadside radiation pattern and peak gain of 5.5 dBi, on a substrate of $0.02\lambda_g$ thickness and patch area $1.44\lambda_g$. Against the reported designs, the current work presents a low profile single patch circularly polarized configuration.

1. INTRODUCTION

Research in wireless communications in recent years has attracted the interest of a broad community, ranging from materials science up to device engineering [1–3, 39]. In wireless applications, to minimize the losses arising from multi-path propagation antennas offering circularly polarized (CP) response are used [1, 2]. Owing to the ease of fabrication and low-profile design, microstrip antenna (MSA) is the preferred option to design CP antennas. Many techniques have been reported to realize CP response using MSA. The CP response in MSAs is realized by cutting a slot inside the patch or by placing a stub on the patch edges [3–9], loading the patch with a shorting post [10], employing parasitic patches in the gap-coupled planar or stacked layer [11–16], using artificial magnetic conductor (AMC) or meta-surface structures [17, 18] by using modified shapes of the radiating patch [19, 20], cutting a resonant slot inside the patch [21, 22], cutting fractal shape slots on the patch or on the ground plane [23–26], and using defected ground plane designs [27–29]. Amongst these techniques, resonant slot cut designs are the optimum one since it is a single patch design and offers axial ratio (AR) bandwidth (BW) of 4–6% with a gain of more than 6 dBi while using substrate thickness of 0.06–$0.08\lambda_g$ As discussed in the comparative study presented in [30], the slot on the ground plane against that on the patch offers better results in terms of BW and frequency reduction. In addition, as a slot placed on the ground plane does not directly affect the modal currents on the patch, it is easier to obtain impedance matching [30]. In the reported literature, simple low profile modified ground plane designs that offer CP response with a moderately high value of the broadside gain are not reported.

In this paper, modified ground plane designs of square MSA (SMSA) and circular MSA (CMSA) are presented on a thinner Arlon substrate ($\varepsilon_r = 3.0$, $\tan\delta = 0.002$, $h = 0.16$ cm), in 2800 MHz frequency band. The defects on the ground plane in the form of fractal shape variations of U-slot and half U-slot are created. The 1st, 2nd, and 3rd order variations of fractal shape slots are studied. Through the parametric study it is noted that the fractal shape slot degenerates patch (SMSA and CMSA) fundamental mode frequency into two orthogonal resonant modes (TM_{10}^{45} and TM_{01}^{135}), which

Received 23 November 2022, Accepted 22 January 2023, Scheduled 6 February 2023
* Corresponding author: Amit A. Deshmukh (amitdeshmukh76@rediffmail.com).
The authors are with the EXTC Department, SVKM's DJSCE, Mumbai, India.

are directed along the patch diagonal axis. An optimum inter-spacing between them yields CP response. On the thinner substrate, all the designs yield impedance BW for $S_{11} \leq -10$ dB of more than 5% and AR BW of 1–2% with the broadside radiation pattern and gain characteristics. Amongst all the fractal shape variations, the CMSA using a 1st order fractal U-slot yields optimum results. It offers AR BW of 60 MHz (2.14%) that lies inside the impedance BW of 162 MHz (5.7%). The MSA shows broadside pattern characteristics with a peak gain of more than 5 dBi. Thus amongst the reported CP variations, the proposed configuration is a low profile design that offers AR BW of more than 2% on a thinner substrate of $0.02\lambda_g$. A detailed comparison of the proposed optimum design against the reported CP MSAs is discussed further in the paper. The configurations presented in this paper are first optimized using IE3D simulations followed by experimental verifications [31]. The MSA is fed using a 50 Ω SMA connector of 0.12 cm inner wire diameter. The experimental validation for the obtained results is carried out inside the antenna lab using instruments like, ZVH–8, FSC 6, and SMB 100 A.

2. DESIGNS OF SMSA BACKED BY FRACTAL SHAPE U-SLOT CUT GROUND PLANE

The design of SMSA backed by fractal shape U-slot variations is shown in Figs. 1(a)–(e). The SMSA dimensions on an Arlon substrate are optimized for TM_{10} mode frequency of 2800 MHz. Thus SMSA

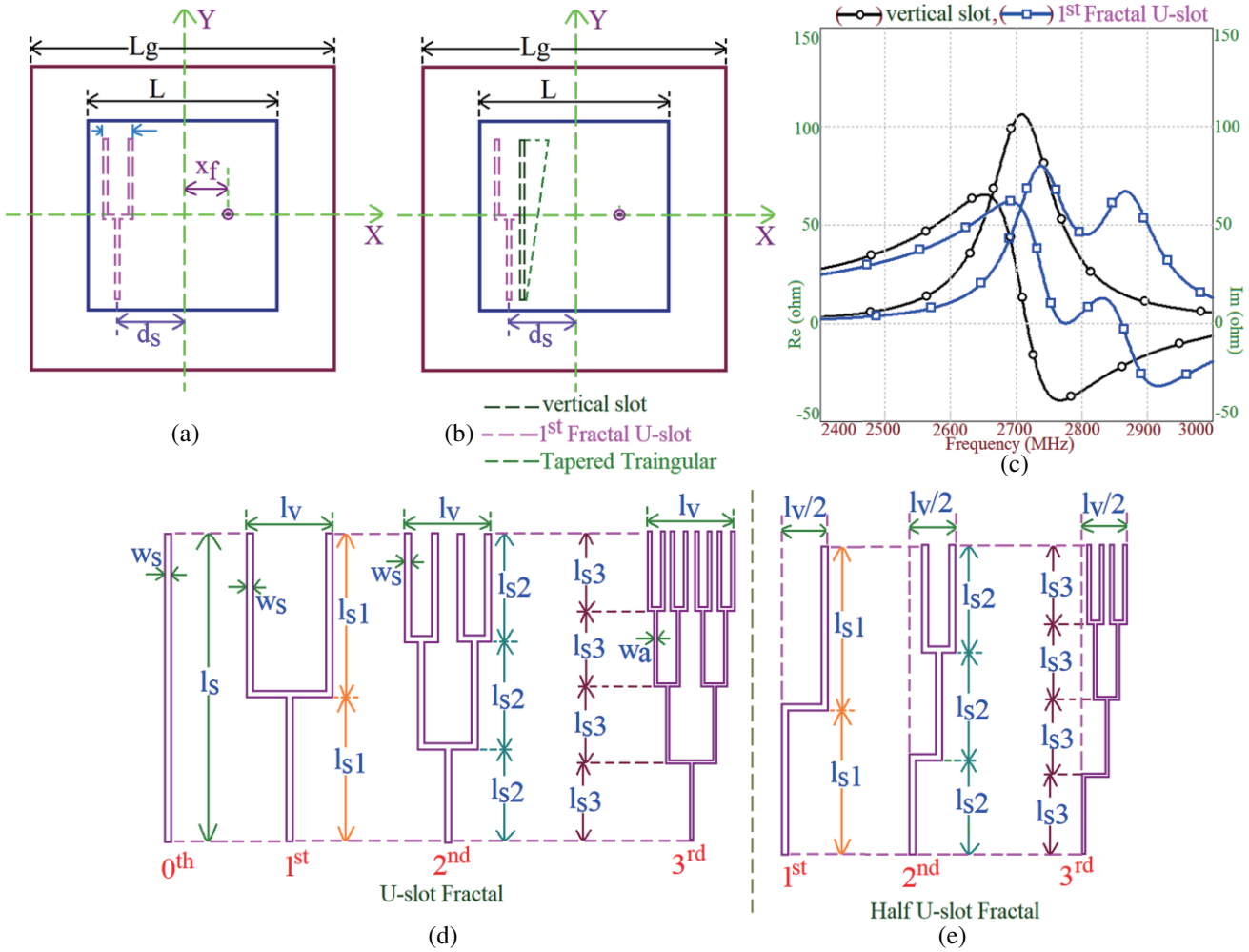

Figure 1. (a), (b) Variations of SMSA backed by fractal and vertical slot cut ground plane, and its (c) resonance curve plots, (d), (e) detailed dimensions of fractal U-slot and half U-slot for a different order.

length is selected as $L = 2.86$. The square ground plane length is taken as $L_g = 4.6$ cm. The feed point is located at a distance of $x_f = 1.0$ cm from the patch center point to excite TM_{10} mode. The fractal variations are placed at a distance 'd_s' cm from the patch center point and on the other side of the coaxial feed. For the feed point shown, excitation of orthogonal mode is not possible to achieve the CP response. Initially, with respect to 1st order fractal variation of the U-slot, a study is carried out that explains how the dual orthogonal modes will be excited in fractal variation against the vertical slot. Resonance curve plots for the same are shown in Fig. 1(c). Using a vertical slot, unequal path lengths along the two diagonal axes on the patch are not realized, whereas due to the fractal U-slot geometry, unequal path lengths are created along two diagonal axes, leading to the two closely spaced resonant modes against the single resonant mode. Tapered width triangular slot as shown in Fig. 1(b) is also studied for the creation of two diagonal orthogonal modes. It is noted in the parametric study that orthogonal modes are created here, but both their frequencies change against the increment in triangular slot dimensions. This does not yield optimum inter-spacing between them to give CP response. Based on these findings, the fractal shape variation of the U-slot is selected.

Initially for the 1st iteration of the fractal U-slot on the ground plane, parametric study for the variation in the position of slot 'd_s' and various slot dimensions, 'l_{s1}', 'l_v', 'w_s', is carried out, and resonance curve plots and surface current distribution at the observed resonant modes are shown in Figs. 2(a)–(d). The position of 1st order fractal U-slot (d_s) for length $l_{s1} = 1.245$ cm is increased from 1.075 to 1.275 cm, away from the patch center. It is noted that for $d_s = 1.075$ cm, a single resonant peak near 2300 MHz is observed. When d_s is increased away from the patch center, a second resonant peak near 2900 MHz is noticed. The frequency of the lower resonant mode increases against an increase in d_s.

The frequency of the higher resonant mode remains nearly constant. The surface currents at lower resonant mode show half wavelength variation along $\phi = 135$ diagonal axis in the square patch, and at higher resonant mode frequency, currents vary along $\phi = 45$. Here, the presence of a fractal U-slot creates unequal current paths along the diagonal axis that degenerate TM_{10} mode into dual orthogonal modes. Because of this diagonal variation, these modes are referred to as TM_{10}^{135} and TM_{01}^{45}, respectively. In defected ground plane MSAs, modifications in modal currents on the ground plane are related to the currents on the patch through the fringing fields between the patch and the ground [30, 33]. Thus with an increase in d_s, perturbations in currents at TM_{10}^{135} mode decrease which increases its frequency, and it comes closer to TM_{01}^{45} mode frequency. This achieves tuning in frequencies of two orthogonal modes. The further optimization of AR value below 3 dB to achieve the CP response is realized by changing fractal U-slot length l_{s1} as shown in Figs. 2(a), (b). The variation in length l_{s1} against further increment in d_s is considered here since the variation in l_{s1} increases the impedance at two orthogonal modes (specifically TM_{01}^{45} mode) to yield an AR value less than 3 dB. Using the parametric study for variation in fractal U-slot parameters on the ground plane, SMSA is optimized for CP response. The antenna parameters in the optimum design for 1st order fractal U-slot variation are, $d_s = 1.275$ cm, $l_{s1} = 0.945$ cm, $l_v = 0.46$ cm, $w_s = 0.1$ cm, $x_f = 1.0$ cm, and results for them are shown in Fig. 2(e). The simulated and measured BWs for $S_{11} \leq -10$ dB are 171 MHz (6.07%) and 178 MHz (6.33%), respectively. The simulated and measured CP BWs for AR < 3 dB are 36 MHz (1.28%) and 41 MHz (1.46%), respectively. Across the AR BW, the antenna offers a gain of more than 5 dBi. The fabricated prototype showing the patch and ground plane is given in Figs. 2(f), (g). The radiation pattern at the center frequency of AR BW and simulated polarization plot at the same are shown in Figs. 3(a)–(c). The radiation pattern is in the broadside direction, with an equal contribution of the co and cross polarization levels. Here as the antenna offers CP radiation, the two levels are nearly the same. The left hand field components are dominant in the polarization plots indicating the presence of left hand CP (LHCP) wave.

The time varying surface current distribution at the center frequency of the AR BW and orthogonal field magnitude (E_x & E_y) and their phase plots (Φ_x–Φ_y) obtained using CST software [32] for 1st order fractal U-slot cut SMSA are shown in Figs. 4(a)–(e). The current vectors rotate in the clockwise direction over time, thus confirming the presence of an LHCP wave. Near the frequency range of 2780 MHz, the magnitudes of E-field vectors, E_x & E_y, are equal. Also at this frequency point Φ_y–Φ_x is nearly around 900. Further, as Φ_y is more than Φ_x, with reference to the time varying fields shown in Fig. 4(e) inset, over the time variation, clockwise rotation of the E-field vector is noted, thereby confirming the

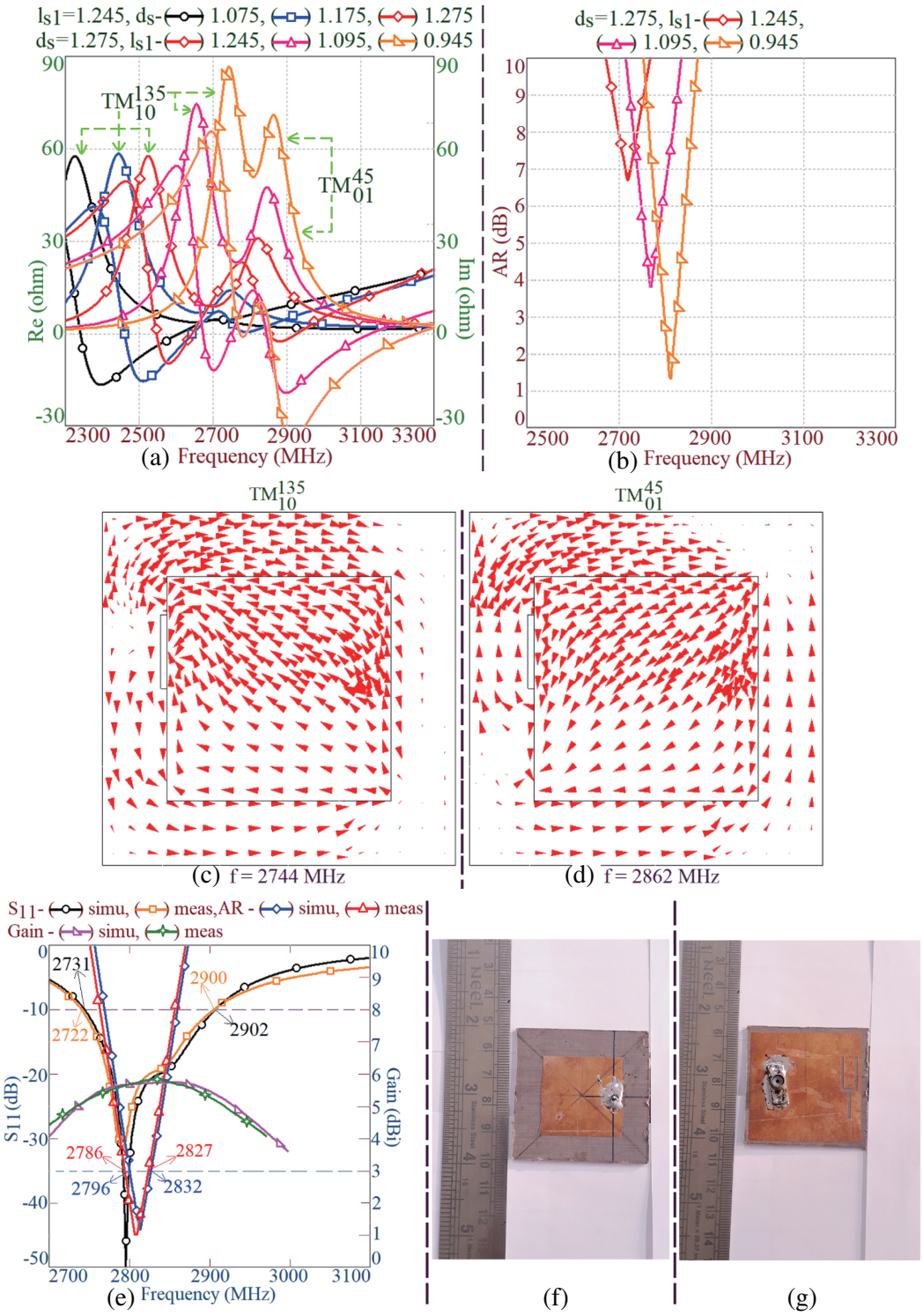

Figure 2. (a) Resonance curve and (b) axial ratio plots for variation in slot position and dimensions, (c), (d) surface current distribution at observed resonant modes, (e) S_{11}, AR BW and gain plots, (f) patch and (g) ground plane views of fabricated antenna for SMSA backed by 1st iteration fractal U-slot ground plane.

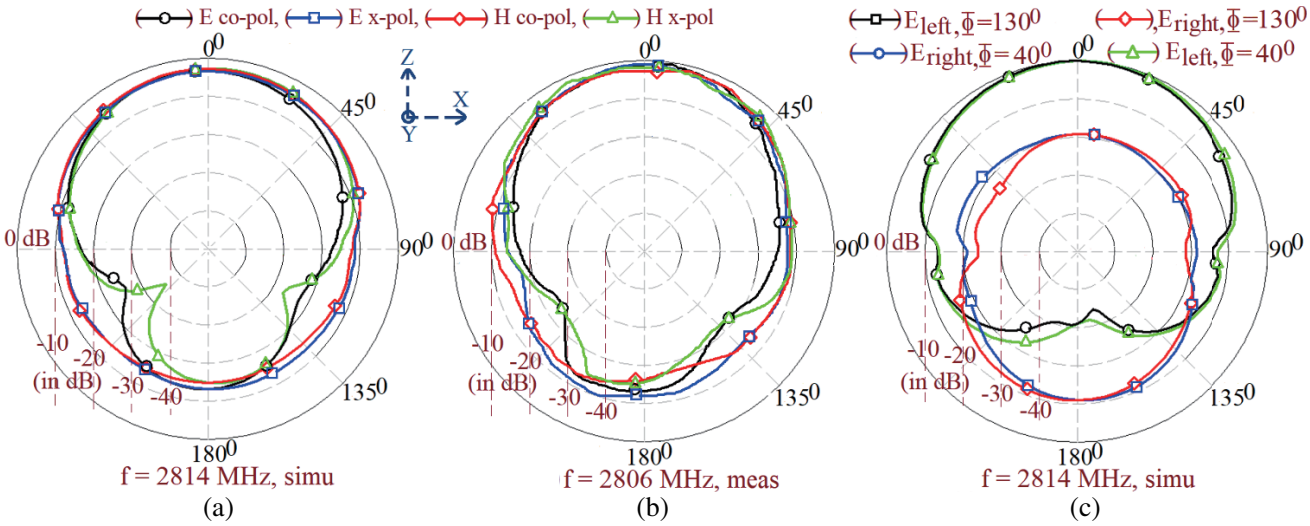

Figure 3. (a), (b) Radiation pattern plots and (c) simulated polarization plots at the center frequency of AR BW for SMSA backed by 1st iteration fractal U-slot cut ground plane.

LHCP radiation. Thus, radiation pattern plots, polarization plots, time varying current distribution, and field magnitude and phase plots confirm the presence of CP radiation. The LHCP radiation is verified experimentally in the lab by using nearly square MSA excited in the LHCP and right hand CP (RHCP) sense of rotation and by observing the received signal. When the senses of polarization in the transmitter and receiver are matched, the received signal is maximum whereas when the sense of polarization is not matched with the antenna under test, then the received signal is reduced by 8–10 dB. This confirms the LHCP response experimentally.

The 2nd and 3rd order fractal variations of the U-slot as shown in Fig. 1(d) are also studied for the CP response. In each design, a parametric study for the variation in slot position and dimensions is carried out to achieve the optimum CP BW. In each fractal variation, the total vertical and horizontal lengths of the fractal U-slot are kept the same, i.e., $2l_{s1} = 3l_{s2}$ and $2l_{s1} = 4l_{s3}$. The fractal horizontal slot length l_v is kept the same in all the fractal orders whereas in the 3rd order fractal variation, U-slot width is selected as $w_a = w_s/2$. The simulated plots of AR BW for 2nd and 3rd order fractal U-slot designs are shown in Fig. 5(a). In the 2nd order fractal design, AR BW is obtained in the same frequency range as that of the 1st order fractal design, whereas in the 3rd order fractal U-slot design, AR BW is obtained in the lower frequency range. As can be noted here that amongst the three order fractal designs, maximum AR BW is obtained in 1st order fractal U-slot variation. Also, 2nd and 3rd order fractal designs are complex in fabrication. Hence, an experimental validation for 2nd and 3rd order fractal U-slot design is not carried out. In the parametric study for d_s, it is noted above that the half portion of the fractal U-slot, which lies below the patch only is responsible for the degeneration of fundamental mode frequency. Hence, instead of a fractal design with U-slot, its half U-slot variation can be explored to yield CP response as shown in Figs. 1(e) and 5(b). To analyze the slot effects, a parametric study for variation in slot parameters is carried out, and resonance curve plots for them are shown in Fig. 5(c). In the design with fractal half U-slot, similar effects in the degeneration of dual frequencies against variation in d_s and l_{s1} to that observed in the design with full U-slot are noted. An optimum response for maximum possible AR BW in 1st order fractal U-slot design is obtained for $L = 2.86$ cm, $L_g = 4.5$ cm, $d_s = 1.275$ cm, $l_{s1} = 0.95$, $w_s = 0.1$ cm, $x_f = 1.0$ cm, and its results are shown in Fig. 5(d).

The simulated and measured BWs for $S_{11} < -10$ dBare 175 MHz (6.12%) and 168 MHz (588%), respectively. The simulated and measured CP BWs for AR < 3 dB are 36 MHz (1.24%) and 4 MHz (1.38%), respectively. Across the AR BW, the antenna offers a gain of above 5 dBi. The fabricated prototype showing the patch and fractal half U-slot cut ground plane is given in Figs. 5(e) and (f). The time varying surface current distribution, radiation pattern plots, and simulated field polarization plots

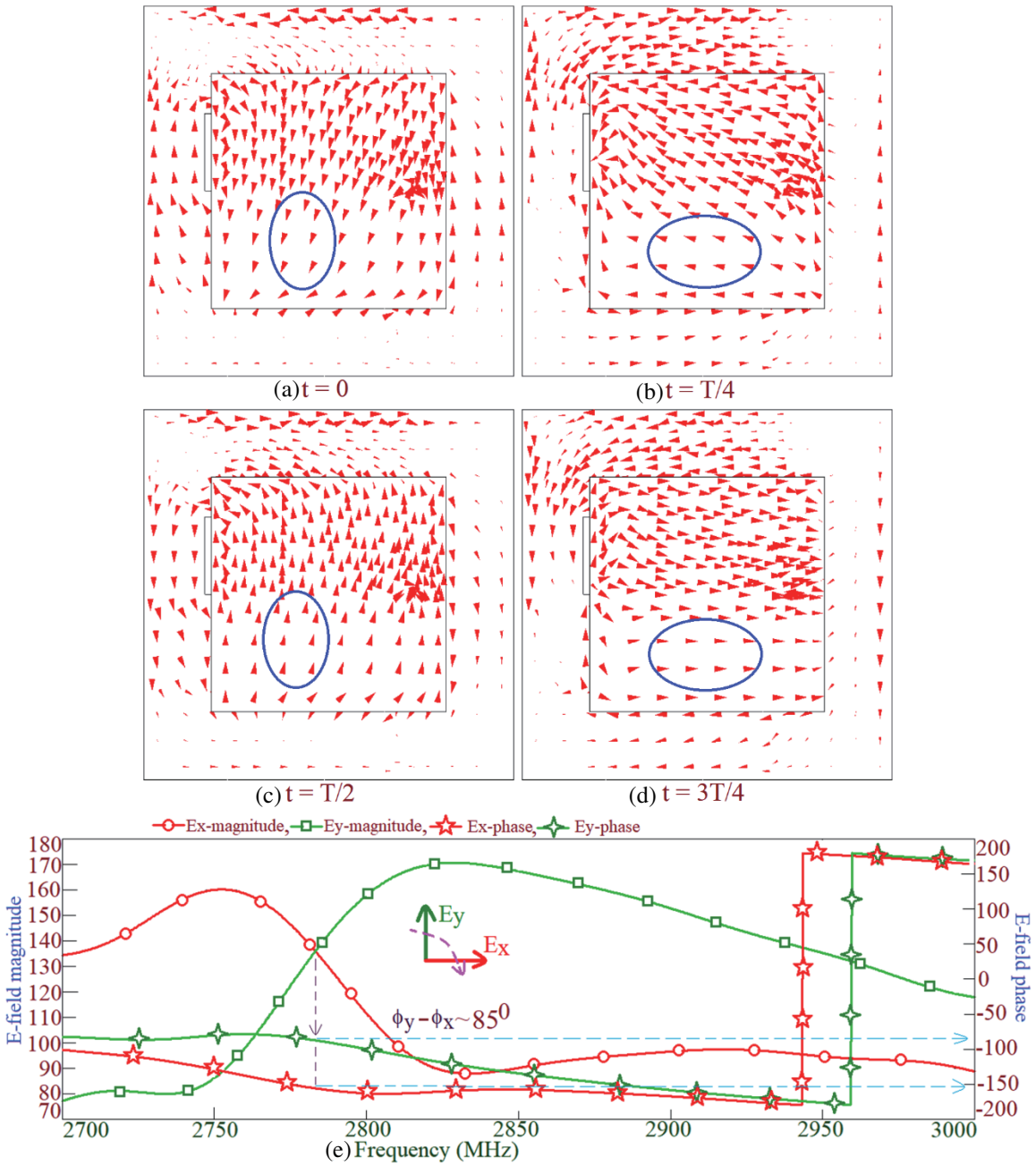

Figure 4. (a)–(d) Time varying surface current distribution at the center frequency of AR BW and (e) orthogonal fields and phase plots for SMSA backed by 1st iteration fractal U-slot cut ground plane.

at the center frequency of AR BW are shown in Figs. 6(a)–(g).

Similar to the above design, current vectors rotate in a clockwise direction against the time indicating the presence of an LHCP wave. This is again confirmed by the polarization plots in which left hand field components are dominant. The pattern is in the broadside direction, and due to the CP response, the co and cross polarization levels are nearly the same observed in the broadside direction. Also in this design, orthogonal field and phase plots were generated using CST software. Similar to the previous design, near the center frequency of the AR band, orthogonal field magnitudes are the same with the phase difference between the two components around 900. The experimental verification of

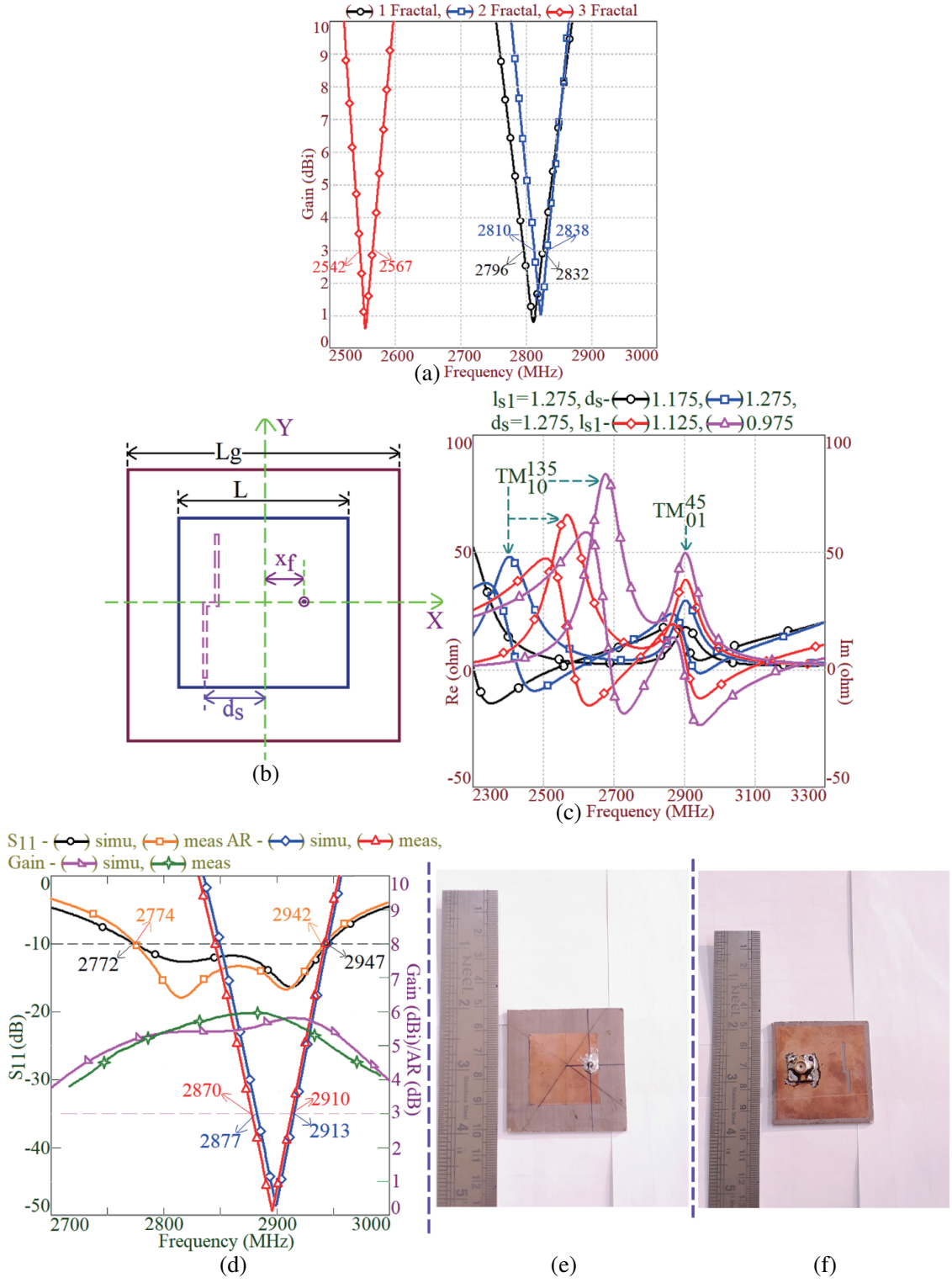

Figure 5. (a) AR BW plots for fractal order variations in U-slot cut ground plane backing SMSA, (b) SMSA backed by 1st order fractal half U-slot and its (c) resonance curve plots for the variation in slot parameters, its (d) results for optimum design and fabricated prototype showing (e) patch and (f) ground plane.

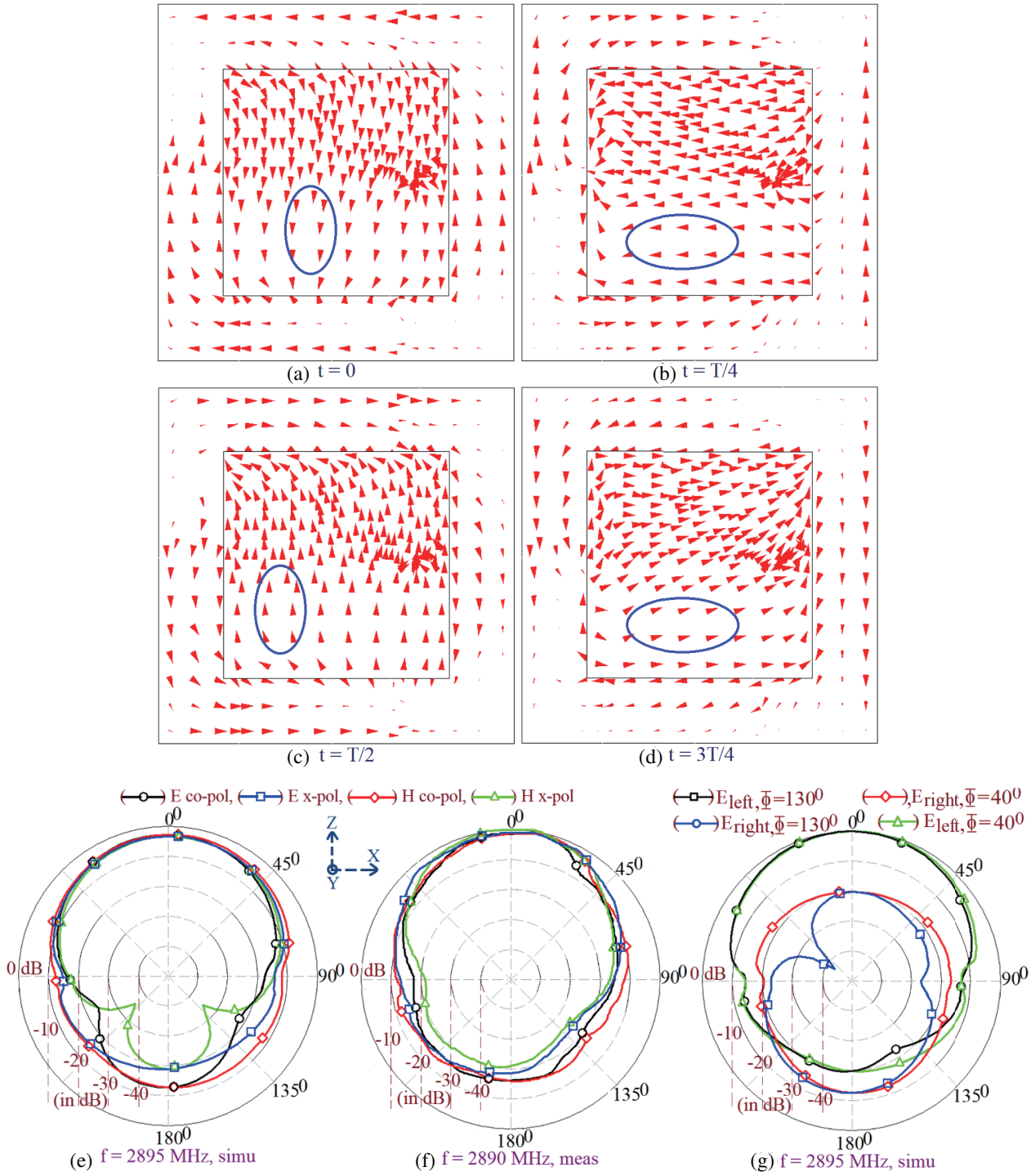

Figure 6. (a)–(d) Time varying surface current distribution, (e), (f) radiation pattern plots and (g) simulated polarization plots at the center frequency of AR BW for SMSA backed by 1st iteration fractal half U-slot cut ground plane.

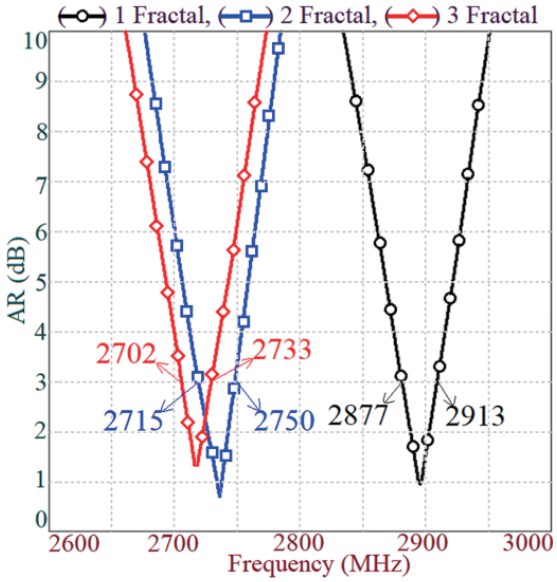

Figure 7. AR BW plots for fractal order variations for SMSA backed by half U-slot cut ground plane.

the sense of rotation is also confirmed in the measurement using the procedure mentioned above, and it shows a similar response. The effects of increasing the order of fractal half U-slot on the ground plane (i.e., 2nd & 3rd order) are also studied, and AR BW plots for the same are shown in Fig. 7. In 2nd and 3rd order fractal half U-slot cut designs, a center frequency of AR BW decreases. Amongst all the designs, 1st order fractal half U-slot cut variation shows optimum result in terms of AR BW.

3. DESIGNS OF CMSA BACKED BY FRACTAL SHAPE U-SLOT CUT GROUND PLANE

In this section, similar designs of CMSA using a fractal variation of either U-slot or half U-slot are studied for CP response as shown in Figs. 8(a) and (b). In each of the designs, a detailed parametric study for the variation in slot position and dimensions for analyzing their effects on the excitation dual orthogonal modes is carried out, in which similar effects are noted. To avoid the repetition of results, resonance curve plots and current distribution for the CMSAs are not given. Through this parametric study, optimum CP designs are obtained, and results for them are provided in Figs. 9–11.

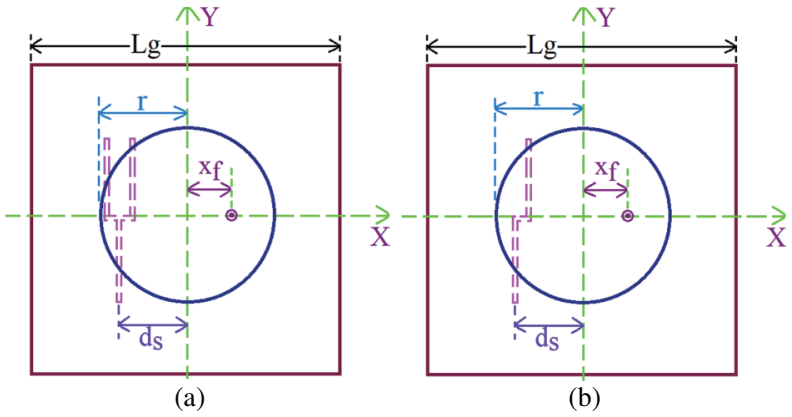

Figure 8. Designs of CMSA backed by fractal variation of (a) U-slot and (b) half U-slot ground plane.

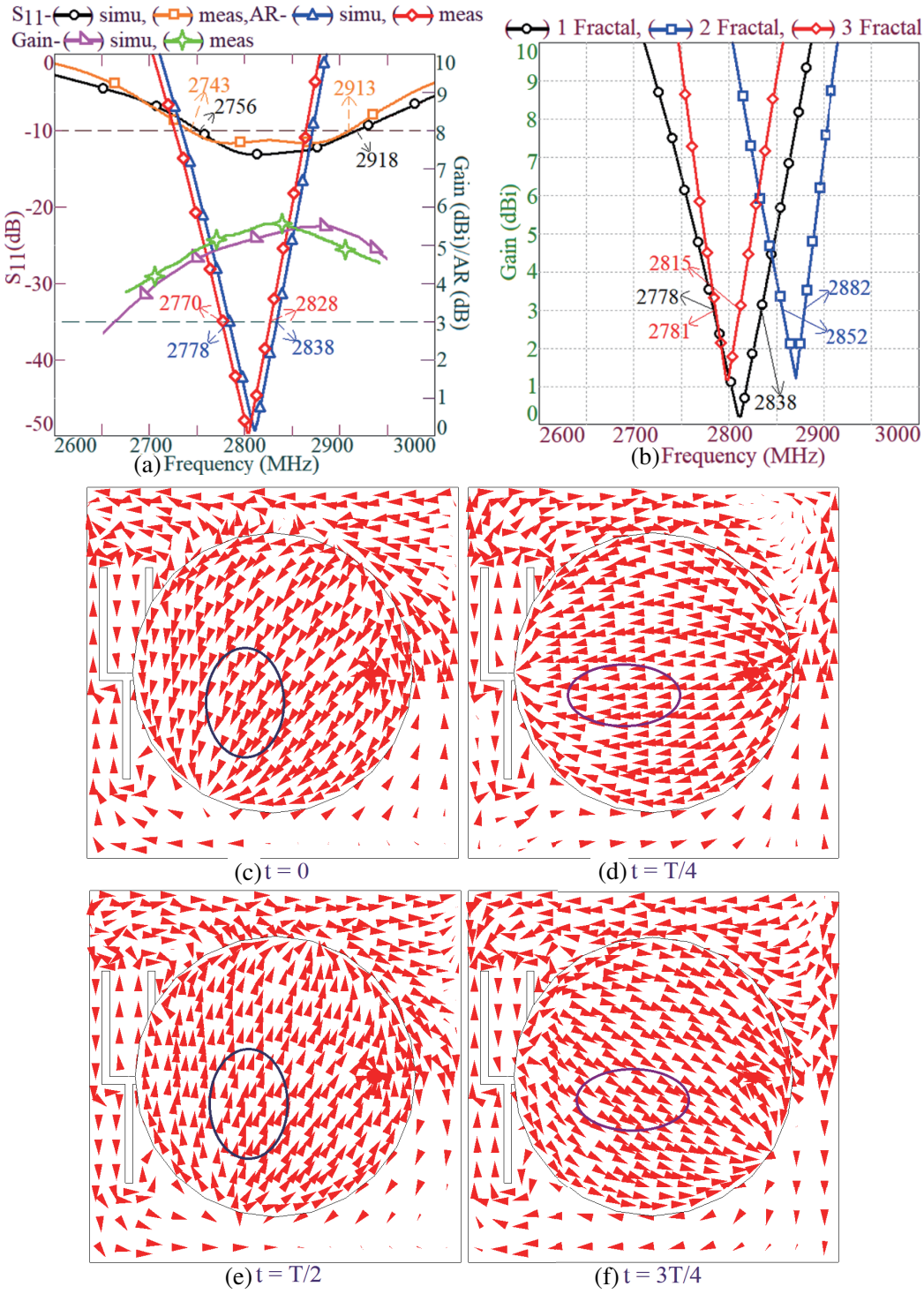

Figure 9. (a) S_{11} & AR BW and gain plots, (b) AR BW plots against variation in fractal order and (c)–(f) time varying surface current distribution at the center frequency of AR BW for CMSA backed by 1st iteration fractal U-slot cut ground plane.

In CMSA with a fractal U-slot, the center frequency of the AR BW changes marginally against the fractal order as shown in Fig. 9(b). The fractal U-slot with 1st order provides an optimum result in terms of AR BW. For the dimensions of the antenna as $r = 1.7\,\text{cm}$, $Lg = 4.5\,\text{cm}$, $ls1 = 1.275\,\text{cm}$,

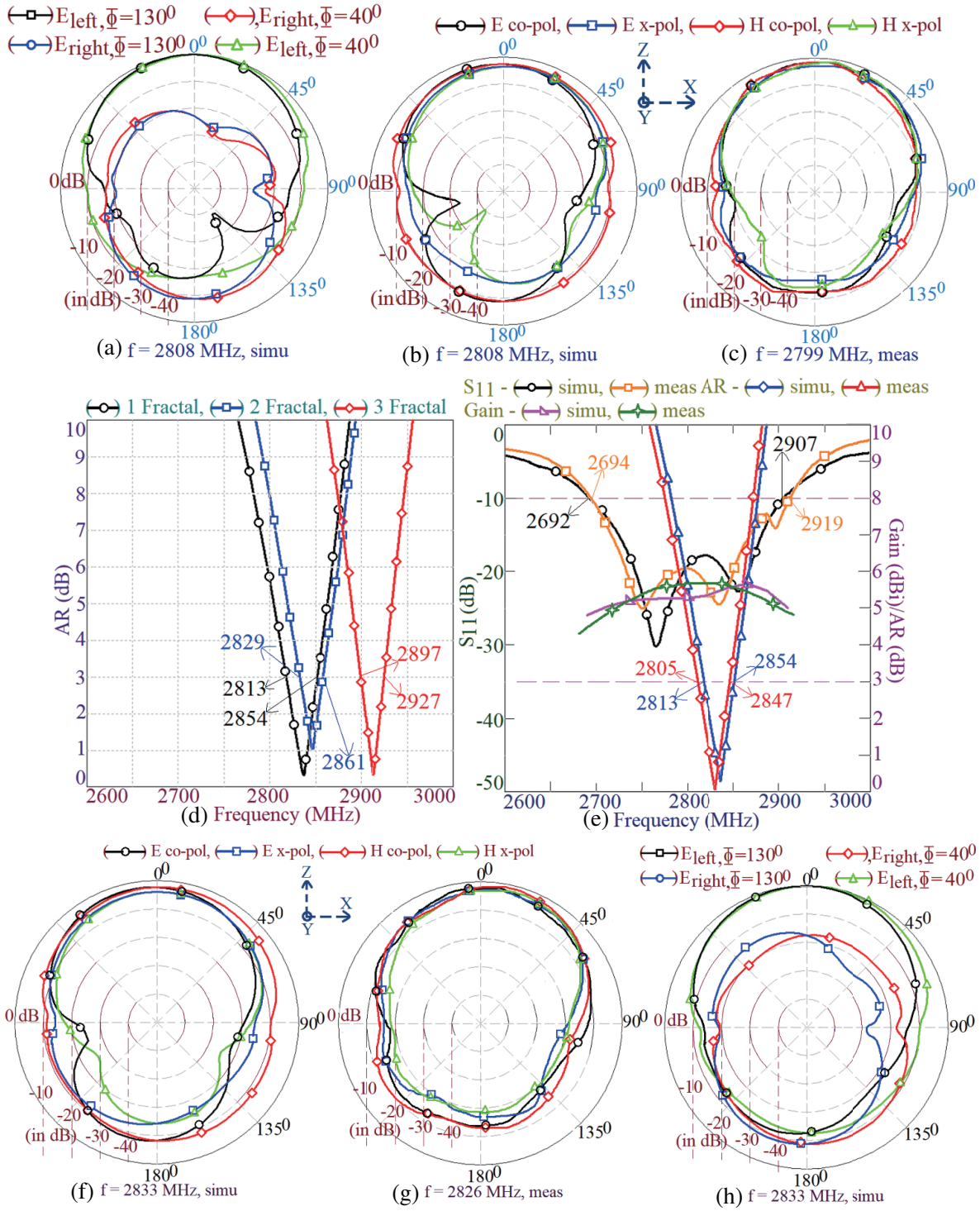

Figure 10. (a), (b) Polarization and (c) radiation pattern plots at the center frequency of AR BW for CMSA backed by 1st order fractal U-slot cut ground plane, (d) AR BW variation against order of the fractal half U-slot cut ground plane, (e) S_{11} & AR BW and gain plots, (f), (g) radiation pattern and (h) polarization plots at the center frequency of AR BW for optimum design of CMSA backed by 1st order fractal half U-slot cut ground plane.

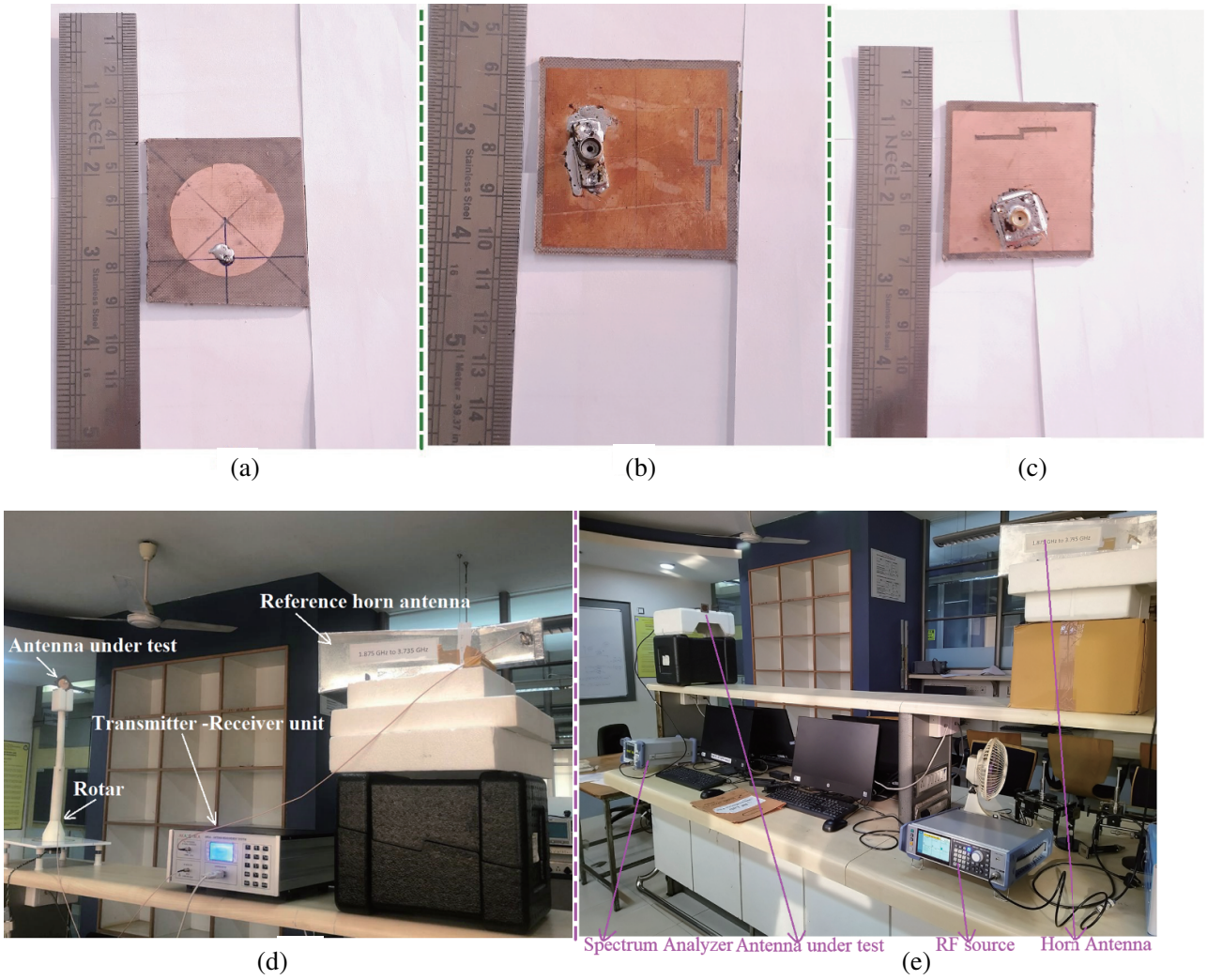

Figure 11. Fabricated antenna showing the (a) CMSA, (b) U-slot and (c) half U-slot cut ground plane, (d) radiation pattern and (e) gain and AR BW measurement setup.

$lv = 0.7\,\text{cm}$, $xf = 1.2\,\text{cm}$, the design with 1st order fractal U-slot variation yields simulated and measured S_{11} BWs of 162 MHz (5.71%) and 170 MHz (6.01%), respectively as shown in Fig. 9(a). The AR BW in the simulation and measurement is 60 MHz (2.14%) and 58 MHz (2.07%), respectively as shown in Fig. 9(a). The broadside gain over the AR BW is more than 5 dBi. The surface currents at the center frequency of AR BW rotate in a clockwise direction over time, thereby indicating the presence of an LHCP wave. This is further confirmed by the simulated field polarization plots, wherein the left hand field components are dominant, as shown in Figs. 10(a)–(c). Radiation pattern at the center frequency of AR BW is in the broadside direction with equal contributions of the co and cross polarization levels.

In the design of CMSA with an increasing order of fractal half U-slot, the center frequency of the obtained AR BW changes marginally as shown in Fig. 10(d). An optimum result in terms of AR BW is obtained in the 1st order fractal half U-slot, and S_{11} & AR BW and gain plots for the same are shown in Fig. 10(e). Here, the simulated and measured S_{11} BWs are 215 MHz (7.68%) and 225 MHz (8.02%), respectively. The AR BW observed in the simulation and measurement is 41 MHz (1.447%) and 42 MHz (1.486%), respectively. Similar to the previous fractal U-slot designs, the antenna offers a broadside gain of more than 5 dBi over the AR BW. The radiation pattern at the center frequency of AR BW is in the broadside direction. Due to the CP nature of radiation, co and cross polarization levels

are nearly the same, in the broadside direction. The polarization field plots show dominant left hand components, indicating the presence of an LHCP wave. This was also confirmed by the time varying current distribution, which shows the rotation of surface currents in clockwise direction against time. As mentioned above, practical validation of the sense of rotation is confirmed by using nearly square MSA excited in LHCP and RHCP sense of rotation as a transmitter. When the senses of rotation between transmitter and receiver match, the received signal strength is maximum.

The E-field magnitude components and their phase plots for the CMSA with 1st order fractal U-slot and half U-slot designs are studied. Near the center frequency of AR BW, they show equal magnitudes of the E_x and E_y components with a phase difference (Φ_y–Φ_x) between them around 900. The fabricated prototype of the CMSA backed by fractal U-slot and half U-slot of 1st order is shown in Figs. 11(a)–(c). The automated radiation pattern and gain and AR measurement setup are shown in Figs. 11(d) and (e). Wideband high gain Horn Antennas were used in the measurement as the reference antennas. In the measurement setup, the largest dimension 'D', which is used in calculating the far field distance is the diagonal length of the horn antenna. Amongst all the proposed designs, by considering the highest frequency of operation, the far field distance ($2D^2/\lambda$) is calculated to be 45 cm. In the pattern and gain measurements, a distance of more than this is considered. The measurement is carried out inside the antenna lab. Around the measurement setup placed on the central desk, no surrounding metal objects are present. In addition, the distance of surroundings objects from the central desk of measurement is more than 8λ and is calculated with reference to the lowest frequency of operation amongst the proposed antenna. This measurement setup ensures minimum reflection from the surrounding objects and thus offers close matching to the measurements being carried out inside an anechoic chamber. The antenna gain is measured using the three antenna method. In the AR BW measurement, as the received signal is in dBm, a difference in the amplitude of the received signals in two polarization is considered, which gives good accuracy. The results for SMSA and CMSA variations are summarized in Tables 1 & 2. Since the measurement is carried out in the optimum case (i.e., 1st order fractal variation), a comparison of simulated results for S_{11} and AR BW is provided. Amongst all the designs, CMSA with 1st order fractal U-slot cut ground plane design provides maximum AR BW. The resonant fields inside the circular cavity are analyzed using the orders of J-type Bessel functions, whereas those inside the rectangular cavity are analyzed using sinusoidal terms [2]. Due to the difference in the field composition, the CMSA design yields higher AR BW than the SMSA when the slots are embedded on the ground plane [2, 3, 33]. Thus, to reflect upon the technical novelty in the proposed circular patch design, the same is compared below against the reported CP MSAs as discussed in the following section.

Table 1. Comparison of SMSA variations backed by different fractal order of U-slot.

Fractal type	Iteration	S_{11} BW, simulated (MHz, %)	AR BW, simulated (MHz, %)
U-slot	1st	171, 6.07	36, 1.28
	2nd	149, 5.26	28, 1.0
	3rd	189, 7.27	25, 0.98
Half U-slot	1st	175, 6.12	36, 1.24
	2nd	238, 8.87	35, 1.28
	3rd	189, 7.27	31, 1.14

4. COMPARATIVE ANALYSIS

The results for CMSA backed by 1st order fractal U-slot cut ground plane variation are compared in Table 3 against the reported CP designs. In the comparison, antenna parameters like AR BW, peak gain, and antenna volume (i.e., patch area and substrate thickness) are considered. As the reported designs are optimized at different frequencies, from the comparison perspective, patch area and substrate thickness are normalized with reference to the center frequency of AR BW. In comparison, some of the

Table 2. Comparison of CMSA variations backed by different fractal order of U-slot.

Fractal type	Iteration	S_{11} BW, simulated (MHz, %)	AR BW, simulated (MHz, %)
U-slot	**1st**	**162, 5.71**	**60, 2.14**
	2nd	255, 8.78	30, 1.05
	3rd	175, 6.15	34, 1.22
Half U-slot	1st	215, 7.68	41, 1.447
	2nd	216, 7.795	32, 1.125
	3rd	376, 12.5	30, 1.03

Table 3. Comparison of CMSA backed by 1st iteration fractal U-slot against reported MSAs.

Configuration reported in Ref	AR BW (MHz, %)	Peak Gain (dBi)	h/λ_{AR}	A_P/λ_{AR}
CMSA U slot 1st iteration	**60, 2.14**	**5.5**	**0.02**	**1.44**
[7]	180, 5.4	10.2	0.086	1.78
[8]	23, 0.925	3.87	0.02	1.51
[9]	40, 1.673	5.0	0.02	4.8
[10]	16, 0.653	7.6	0.04	3.5
[11]	1400, 22.76	8.5	0.281	7.585
[12]	40, 3.4	5.6	0.034	3.125
[13]	1400, 11.57	5.25	0.135	0.13
[14]	1510, 27	8.74	0.14	4.868
[15]	100, 3.3	2.7	0.034	5.4
[16]	129, 14.27	7.6	0.14	9.2
[17]	48, 5.25	1.87	0.02	17.85
[19]	46, 3.9	3.45	0.01	4.97
[20]	79, 6.4	8.5	0.108	> 3
[21]	130, 5.3	9.0	0.101	2.362
[22]	1000, 19	7.5	0.12	3.54
[23]	50, 1.45	8.36	0.076	4.0
[24]	26, 1.084	4.62	0.026	1.285
[25]	32, 2.13	5.9	0.025	1.588
[26]	6, 0.4	2.2	0.053	1.358
[27]	42.6, 1.8	7.9	0.026	0.858

references deal with multi-band design, in which comparison is presented with reference to their first band of operation. In the design reported in [5], multiple slots and stubs are used. In spite of these modifications, achieved AR BW is less than 1%. In the CP design discussed in [6], although obtained AR BW is $> 3\%$, the configuration employs dual patches with differential feeding and a defected ground plane structure. These together increases the design complexity. The MSA presented in [7] offers a gain of > 10 dBi, but the substrate thickness is large. The design reported in [8] offers a wide beam width CP response but gives AR BW less than 1% with a less gain. The E-slot loaded design in [9] although offers

comparable values of AR BW and gain, it requires a larger patch size. Using shorting post wideband CP design is reported in [10]. The loading of shorting post on the patch alters the resonant modes of the antenna cavity [3]. Hence, the shorted patch modes here that offer reported wideband CP response are not discussed in [10]. In the CP designs employing parasitic patches [11–16], either the antenna size is larger or the substrate thickness is higher. Here either of the two increases the antenna volume. The CP designs employing an AMC structure increase the antenna size and design complexities [17, 18]. The planar CP design reported in [19] employs a meshed ring structure. Apart from the design complexities presented here, the antenna reported in [19] requires a larger patch size. The modified patch shape design discussed in [20] requires a larger patch size and antenna thickness. The resonant slot cut CP designs require higher substrate thickness [21, 22]. The CP fractal designs discussed in [23] need a larger patch size, whereas the design in [24] employs a complex tree shape fractal design. The fractal design discussed in [25] employs a multi-layer design with a slot on the patch, feeding using a microstrip line and the 2nd order of the fractal slot. Against this proposed design is a single layer coaxial feed design. The fractal SMSA design discussed in [26] offers a smaller AR BW than the proposed design. Further, all the reported fractal CP variations [23–26] employ higher order of the fractal slot. Against them the proposed design employs first order fractal slot and offers higher AR BW. The CP design discussed in [27] employs a slot on the patch as well as the ground plane, whereas AR BW is smaller and obtained over the UWB range for the design discussed in [28]. The design presented in [29] employs multiple slots on the ground and bend strip. These together increases the design complexity. In addition, the patch resonant modes that contribute to the realized AR BW are not discussed in [29]. The slot cut design reported in [34] offers AR BW in the range of 2–3%, but offers lower gain and requires thicker substrate ($h > 0.05\lambda_g$). The CP design discussed in [35] employs a multi-layer structure that increases design complexities. The dual band design for CubeSat application presented in [36] offers AR BW lower than 1% in the two operating bands. The design for a similar application reported in [37] employs slots on the patch as well as the ground plane, which increases the design complexity. The modified slot cut design discussed in [38] offers AR BW less than 1%.

5. CONCLUSIONS

Designs of square and circular shape microstrip antennas using 1st, 2nd, and 3rd order fractal variations of U-slot and half U-slot cut on the ground plane are proposed for single band CP response. The fractal slots on the ground plane degenerate patch fundamental mode into dual orthogonal modes, and an optimum inter-spacing between them yields CP response. Amongst all the designs, CMSA backed by 1st order fractal U-slot cut ground plane offers optimum results. It yields 2.14% of AR BW with a peak broadside gain greater than 5 dBi but on the substrate with thickness and patch area of 0.02λ and 1.44λ, respectively. Against the reported fractal slot cut variations the proposed design offers CP response with 1st order thereby reducing the design complexities. In terms of AR BW, gain, and antenna volume, the proposed design offers better results than the reported configuration and thus provides a low profile design option.

REFERENCES

1. Balanis, C. A., *Antenna Theory & Design*, 3rd Edition, John Wiley & Sons Inc., 2005.
2. Garg, R., P. Bhartia, and I. Bahl, *Microstrip Antenna Design Handbook*, Artech House, London, 2001.
3. Kumar, G. and K. P. Ray, *Broadband Microstrip Antennas*, 1st Edition, Artech House, USA, 2003.
4. Wong, K. L., *Compact and Broadband Microstrip Antennas*, 1st Edition, John Wiley & Sons, Inc., New York, USA, 2002.
5. Heidari, A. A., M. Heyrani, and A. Nakhkash, "Dual band circularly polarized stub loaded microstrip patch antenna for GPS applications," *Progress In Electromagnetics Research*, Vol. 92, 195–208, 2009.
6. Jamal, M. Y, M. Li, and K. L. Yeung, "Isolation enhancement of closely packed dual circularly polarized MIMO antenna using hybrid technique," *IEEE Access*, Vol. 8, 11241–11247, 2020.

7. Hao, S., Q. Chen, J. Li, and J. A. Xie, "High-gain circularly polarized slotted patch antenna," *IEEE Antennas and Wireless Propagation Letters*, Vol. 19, No. 6, 1022–1026, 2020.
8. Ray, M. K., K. Mandal, and N. Nasimuddin, "Low-profile circularly polarized patch antenna with wide 3 dB beamwidth," *IEEE Antennas and Wireless Propagation Letters*, Vol. 18, No. 12, 2473–2477, 2019.
9. Bernard, L. B. K., Nasimuddin, and A. Alphones, "An E-shaped slotted-circular patch antenna for circularly polarized radiation and radiofrequency energy harvesting," *Microwave and Optical Technology Letters*, Vol. 58, No. 5, 868–875, 2016.
10. Zhang, X., L. Zhu, and N. Liu, "Pin-loaded circularly-polarized patch antennas with wide 3-dB axial ratio bandwidth," *IEEE Transactions on Antennas and Propagation*, Vol. 65, No. 2, 521–528, 2017.
11. Dia, W. J. and Z. F. Huang, "A broadband circularly polarized stacked microstrip patch antenna with parasitic elements," *International Journal of RF and Microwave Computer-Aided Engineering*, Vol. 32, No. 8, 1–8, 2021.
12. Falade, O. P., M. U. Rehman, Y. Gao, X. Chen, and C. G. Parini, "Single feed stacked patch circular polarized antenna for triple band GPS receivers," *IEEE Transactions on Antennas and Propagation*, Vol. 60, No. 10, 4479–4484, 2012.
13. Dash, S. K, Q. S. Qingsha, T. Cheng, and T. Khan, "An off-center-fed compact wideband antenna with truncated corners and parasitic patches for circular polarization," *International Journal of RF and Microwave Computer-Aided Engineering*, Vol. 30, No. 8, 1–10, 2020.
14. Jagtap, S. D., R. Thakare, and R. K. Gupta, "Low profile, high gain and wideband circularly polarized antennas using hexagonal shape parasitic patches," *Progress In Electromagnetics Research C*, Vol. 95, 15–27, 2019.
15. Lin, J. and Q. Chu, "Enhancing bandwidth of CP microstrip antenna by using parasitic patches in annular sector shapes to control electric field components," *IEEE Antennas Wireless Propagation Letters*, Vol. 17, No. 5, 924–927, 2018.
16. Sim, C. Y. D., Y. W. Hsu, C. W. Lin, and G. Yang, "Broadband circularly polarized antenna with moon-shaped parasitic element," *International Journal of RF and Microwave Computer-Aided Engineering*, Vol. 26, No. 5, 387–395, 2016.
17. Sarkar, S. and B. Gupta, "A dual-band circularly polarized antenna with a dual-band AMC reflector for RFID readers," *IEEE Antennas and Wireless Propagation Letters*, Vol. 19, No. 5, 796–800, 2020.
18. Sheersha, J. A., N. Nasimuddin, and A. A, Alphones, "High gain wideband circularly polarized antenna with asymmetric meta-surface," *International Journal of RF and Microwave Computer-Aided Engineering*, Vol. 29, No. 7, 1–9, 2019.
19. Agrawal, N. and A. K. Gautum, "Design of low volume circularly polarized annular ring-shaped planar antenna for GPS applications," *International Journal of RF and Microwave Computer-Aided Engineering*, Vol. 31, No. 4, 1–12, 2021.
20. Deshmukh, A. A. and K. P. Ray, "Circularly polarized designs of modified isosceles triangular microstrip antennas," *Engineering Reports*, Wiley Publication, (https://onlinelibrary.wiley.com/doi/10.1002/eng2.12250).
21. Kovitz, J. M., R. Harish, and R.-S. Yahya, "Circularly polarised half E-shaped patch antenna: A compact and fabrication-friendly design," *IET Microwave Antennas and Propagation*, Vol. 10, No. 9, 932–938, 2016.
22. Mondal, T., M. Sandip, G. Rowdra, and B. C. S. Ranjan, "Design and analysis of a wideband circularly polarized perturbed psi-shaped antenna," *IET Microwaves, Antennas & Propagation*, Vol. 12, No. 9, 1582–1586, 2018.
23. Vijayankutty, R., M. Abraham, P. Parvathy Ambalath, and M. Thomaskutty, "Multiband circularly polarised microstrip patch antenna with Minkowski fractal slot for wireless communications," *Progress In Electromagnetics Research C*, Vol. 116, 65–80, 2021.
24. Pandey, S. K, G. P. Pandey, and P. M. Sarun, "Circularly polarized microstrip antenna with fractal trees loaded ground plane," *Electromagnetics*, Vol. 39, No. 7, 505–523, 2019.

25. Prajapati, P. R., G. K. Murthy, A. Patnaik, and M. V, Kartikeyan, "Design and testing of a compact circularly polarized microstrip antenna with fractal defected ground structure for L-band applications," *IET Microwaves, Antennas and Propagation*, Vol. 9, No. 11, 1179–1185, 2015.
26. Wei, K., J. Y. Li, L. Wang, R. Xu, and Z. J. Xing, "A new technique to design circularly polarized microstrip antenna by fractal defected ground structure," *IEEE Transactions on Antennas Propagation*, Vol. 65, No. 7, 3721–3725, 2017.
27. Shinde, J. P., R. Kumar, and M. D. Uplane, "Circularly polarization in defected hexagonal shaped microstrip antenna," *Wireless Personal Communications*, Vol. 75, No. 2, 843–856, 2014.
28. Maurya, R. K., B. K. Kanaujia, A. K. Gautam, S. Chatterji, and A. K. Singh, "Circularly polarized hexagonal ring microstrip patch antenna with asymmetrical feed and DGS," *Microwave and Optical Technology Letters*, Vol. 62, No. 4, 1–7, 2019.
29. Jhajharia, T. and V. Tiwari, "Polarisation reconfigurable dual-band circularly polarised patch antenna with defected ground plane for C-band wireless applications," *IET Microwaves, Antennas & Propagation*, Vol. 13, No. 14, 2551–2558, 2019.
30. Kadam, P. A. and A. A. Deshmukh, "Variations of compact rectangular microstrip antennas using defected ground plane structure: Compact rectangular microstrip antennas," *Journal of Microwaves Optoelectronics and Electromagnetic Applications*, Vol. 21, No. 2, 265–283, 2022.
31. IE3D software, Version 12.
32. CST Software, Version 2019.
33. Guha, D. and Y. M. M. Antar, *Microstrip and Printed Antennas New Trends, Techniques and Applications*, Wiley & Sons publication, 2011.
34. Darimireddy Naresh, K., R. Ramana Reddy, and A. Mallikarjuna Prasad, "Asymmetric triangular semi-elliptic slotted patch antennas for wireless applications," *Radioengineering*, Vol. 27, No. 1, 85–93, 2018.
35. Wei, Z., H. Zhai, S. Ma, D. Yang, and K. Xue, "A low-profile broadband circular polarization filtering antenna," *Microwave and Optical Technology Letters*, Vol. 60, No. 12, 3029–3033, 2018.
36. Lee, S., S. Pyo, and J.-H. Kim, "Dual-band bidirectional circularly polarized microstrip antenna for CubeSat system," *Microwave and Optical Technology Letters*, Vol. 60, No. 12, 2989–2992, 2018.
37. Lee, S., S. Pyo, and J.-H. Kim, "Circularly polarized microstrip antenna with bidirectional radiation using dual-layered arrow-shape slot perturbation for CubeSat application," *Microwave and Optical Technology Letters*, Vol. 60, No. 8, 2018–2022, 2018.
38. Sung, Y. J., "Circularly polarized Mercedes-Benz logo antenna for GPS applications," *Microwave and Optical Technology Letters*, Vol. 58, No. 10, 2308–2311, 2016.
39. Chaccour, C., M. N. Soorki, W. Saad, M. Bennis, P. Popovski, and M. Debbah, "Seven defining features of terahertz (THz) wireless systems: A fellowship of communication and sensing," *IEEE Communications Surveys & Tutorials*, Vol. 24, No. 2, 967–993, 2022.